Effect of TiO_2 addition on Al_2TiO_5 (tialite) phase evolution of *in situ* $MgAl_2O_4$ formation zero cement castable (ZCC)

Y. Kalpaklı*

In this study, densification behaviour of the *in situ* $MgAl_2O_4$ formation zero cement castable (ZCC) in the presence of TiO_2 was analysed. Using a 2 wt-% content of TiO_2 increased the bulk density of the brick to 3·10 g cm^{-3} and decreased the porosity to ~15·7%. Alternatively, a 2 wt-% TiO_2 addition modified the firing shrinkage. X-ray diffraction (XRD) analysis of the fired samples demonstrated that $MgAl_2O_4$ spinel and Mg_2TiO_4 inverse spinel structures also formed, as well as the formation of Al_2TiO_5 in 2 wt-% TiO_2 addition of castables. The SEM investigations of fired samples were carried out to compare the effect of TiO_2 addition and *in situ* phase formation on the physicomechanical properties of castables. The effect of TiO_2 content on the mechanism of the slag penetration of ZCC for a steel ladle was examined, and the penetration layer was chemically analysed.

Keywords: Electron microscopy, X-ray diffraction, Mechanical characterisation, *In situ* spinel, Al_2TiO_5 (tialite), Slag penetration

Introduction

The thermal expansion behaviour of Al_2O_3–MgO castables is related to the spinel formation reaction, which is affected by both temperature and MgO content. Owing to the volume expansion associated with the *in situ* spinel formation reaction from MgO and Al_2O_3, Al_2O_3–MgO, castables show different microstructures and properties compared to those seen in Al_2O_3 spinel castables. On the other hand, the effects of additives on the sintering of spinel powders have also been extensively studied. It is commonly accepted that addition of appropriate amounts of TiO_2 can significantly increase spinel densifications.[1] TiO_2 can influence sintering by forming liquid phase that interact with other components present in the system. In addition, TiO_2 acts as a nucleating agent, recrystallising the magnesium aluminium silicate type liquid phases, with further formation of secondary MgO–Al_2O_3 spinel.[2–4] Increasing TiO_2 from 0 to 1·5% gradually increases the sintered density believed due to exsolution of alumina and dissolution of TiO_2.[1]

According to Hasselman, the combination of Al_2O_3 and TiO_2 leads to the formation of β-Al_2TiO_5 (tialite) that exhibits the highest R_1 thermal shock parameter of all ceramics.[5]

Aluminium titanate is known as an excellent refractory material for use at demanding high temperature applications because it has a low thermal expansion coefficient ($0{\cdot}2–1\times10^{-6}$ K^{-1}) (in this way excellent thermal shock resistance), low thermal conductivity (0·9–1·5 W m^{-1} $°C^{-1}$), low Young's modulus and a high melting point (1860°C).[6,7] A low thermal expansion coefficient and low Young's modulus of elasticity improve the thermal shock performances.[8] Hasselman has illustrated the effect of thermal shock on the strength of ceramics, and the regions of applicability of the various thermal stress fracture parameters.[9] Moreover, Al_2TiO_5 ceramics have very low thermal expansion because of microcracks at grain boundaries induced by the high anisotropy along their three crystallographic axes,[10] but also, microcracks are responsible for the mechanical weakness of the material. Because of its tendency to decompose to α-Al_2O_3 (corundum) and TiO_2 (rutile) at temperatures between 800 and 1280°C, which leads to extensive microcracking during cooling,[11] the industrial applications of this material are limited. It is known that several additives (MgO and Fe_2O_3) may help reduce the rate of decomposition and increase the strength and conversion of Al_2TiO_5.[12,13] The oxides are used as an additive that forms solid solutions with the aluminium titanate.[13]

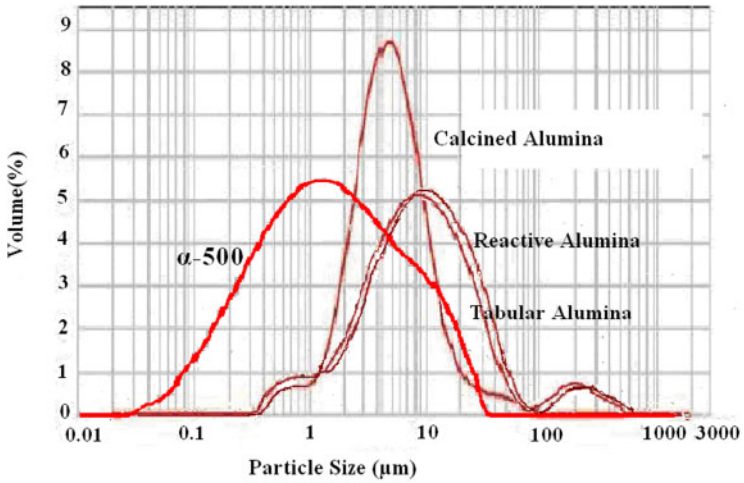
However, the formation mechanism of the Al_2TiO_5 has not been clearly explained up until now. No consensus has existed about the role of the transitional phases during the synthesis process. However, it is reported by Buscaglia that the transitional phase plays an important role during the formation of Al_2TiO_5, when it proceeds in the presence of the MgO by Buscaglia.[14,15] This transitional phase is mentioned by Buscaglia as an identifiable $MgTi_2O_5$.

Al_2TiO_5 and $MgTi_2O_5$ can be described in the pseudobrookite group Ti oxide.[16] The cation disorder between the two nonequivalent octahedral site depends on temperature, composition and, probably, pressure, and it

Faculty of Chemistry and Metallurgy, Department of Chemical Engineering, Yildiz Technical University, Istanbul, Turkey

*Corresponding author, email kalpakli@yildiz.edu.tr

© 2014 Institute of Materials, Minerals and Mining
Published by Maney on behalf of the Institute
Received 9 January 2014; accepted 23 March 2014
DOI 10.1179/1743676114Y.0000000161



1 Particle size distribution of tabular alumina, reactive alumina, calcined alumina and α-500 hydratable alumina

strongly affects the physical and chemical properties of both end members and solid solution.

Xirouchakis showed the configuration entropy variation in $MgTi_2O_5$ as a function of cation disorder with temperature. In other words, $R_2^{3+}TiO_5$ (Al_2TiO_5) solutions may reach entropy maxima at lower temperatures than $R^{2+}Ti_2O_5$ ($MgTi_2O_5$) solutions, or the configurational entropy of $R_2^{3+}TiO_5$ solutions is greater than that of $R^{+2}Ti_2O_5$ solutions at the same temperature.[17]

Huang *et al.*[18] explained that the $MgAl_2O_4$ phase is detected between 1000 and 1220°C. However, the maximum decomposition rate of Al_2TiO_5 is in the temperature range of 1100–1150°C, and in >1280°C, no decomposition takes place. During the formation of $MgAl_2O_4$, one type of Al_2TiO_5–$MgTi_2O_5$ solid solution may occur.[19]

Kalpakli[20] studied the effect of the MgO ratio on the reaction sintered of the *in situ* $MgAl_2O_4$ spinel zero cement refractory castable (ZCC). The optimum MgO ratio was determined as 6 wt-% at a 1600°C sintering temperature. Moreover, it was determined that a 0·1% volume expansion occurred.

Most works in the field specified that TiO_2 addition stabilised the Al_2O_3–MgO spinel. This study aims at improving the performance of Al_2O_3–MgO spinels in ZCC at high temperature in air atmosphere. The densification effect was examined by measuring the apparent density, open porosity and phase composition and by evaluating the microstructure of sintered castable. Moreover, in the present study, the influence of the Al_2TiO_5 (Tialite) phase on the effects of slag penetration of *in situ* $MgAl_2O_4$ formation new generation ZCC prepared using tabular alumina, reactive alumina, calcined alumina and sea water magnesia with 6 wt-% and α-500 hydratable alumina binder, was investigated.

Experimental

Properties of raw materials

In this work, alumina of various particle sizes produced by Almatis Industrial Chemicals (Germany) was mixed with sea water magnesia (origin of China) to form a blend. α-500 hydratable alumina was used as a binder.

X-ray fluorescence analysis of sea water magnesia was conducted in a Spectro-IQ2 system using Breıtlander Autofluxer fusion equipment. These analysis results are given in Table 1 as a chemical composition of sea water magnesia and hydratable alumina.

The particle size distributions of tabular alumina, reactive alumina, calcined alumina and α-500 hydratable alumina was measured in a Malvern Mastersizer 2000 (Malvern, Germany) instrument. These analysis results are given in Fig. 1.

TiO_2 can exist in three crystalline forms: brookite (orthorhombic), rutile (tetragonal) and anatase (tetragonal). TiO_2 used in this study were obtained from Merck. The purity is >99%, and the powder size is <40 μm.

TiO_2 in rutile crystalline form at different proportions was added to the batches as a powder form (the composition are given in Table 2).

Preparation of samples

The mixtures were prepared using basic materials, whose particle size distribution is given in Table 2.

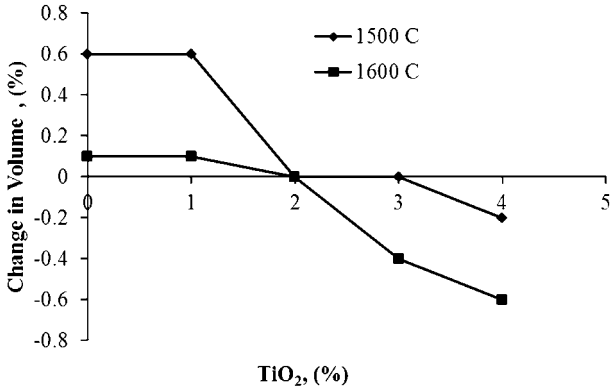
Mixtures of the castable composition given above included sea water magnesia fine powder aggregates, alumina including tabular, reactive and calcined (various particle size distributions) and α-500 hydratable alumina binder as well as the TiO_2 as an additive.

Various additions of TiO_2 (1, 2, 3 and 4 wt-%TiO_2, given the following identification T1, T2, T3 and T4) were added to the mixtures listed in Table 2.

Each mixture was first dry mixed in a Hobart A200 mixer for 2 min. Afterwards, the premixed slurry of

Table 1 Chemical composition of sea water magnesia and hydratable alumina

Raw material	Composition/%	
Sea water magnesia	MgO	98·8
	Al_2O_3	0·054
	SiO_2	0·09
	CaO	0·065
	Fe_2O_3	0·22
	Cr_2O_3	0·08
	Na_2O	<0·11
α-500 hydratable alumina	Al_2O_3	83·0
	CaO	0·60
	Na_2O	0·30
	SiO_2	0·30
	Physical properties	
	Lost of humidity (% 25–250°C)	6·50
	Lost of mass (% 250–1100°C)	9·20



2 Variation of volume in change (%) with TiO_2 (%) addition

blend was added to water, and wet mixing was carried out for ~5 min. The homogenised mixture was cast into moulds of $5 \times 5 \times 5$ cm onto a vibrating table with a 50 Hz vibrating rate. The samples were kept for 24 h at room temperature for 1 day and then cured at a temperature of 110°C for 24 h in Binder type incubator. The refractory samples were sintered in two different groups at a temperature of 1500 and 1600°C for 5 h in Naber Therm, Germany type controlled direct heater furnace at a heating speed of 5°C min^{-1}.

After firing, porosity and bulk density, cold crushing strength (CCS) and slag tests were carried out. The apparent porosity and bulk density were measured by the water immersion method according to the DIN 51056 standard. The CCS tests were carried out according to the DIN 51067 standard. The CCS tests were carried out in a 200 t hydraulic press (Atom Technique, Turkey).

X-ray diffraction experiments were conducted with Philips PANalytical X'Pert PRO X equipment using a setting of 45 mA and 40 kV at a 2θ range between 0 and 90°.

The scanning electron microscopy (SEM) investigations were carried out in JEOL T-330 SEM operated at 20 kV, and linked with a Noran energy dispersive spectrometer (EDS) attachment

Results and discussion

Effect of TiO_2 addition on physical and mechanical properties of ZCC

Figure 2 shows that no improvement occurred in the 1 wt-%TiO_2 added sample sintered at 1500°C in the change in the volume expansion equal to 0·6% that occurred in the case of the non-added sample, no change in size was observed in 2 and 3 wt-%TiO_2 added samples before and after sintering and a firing shrinkage occurred equal to 0·1% that occurred upon addition of 4 wt-%TiO_2. However, no improvement was observed in the 1 wt-%TiO_2 added sample sintered at 1600°C in the change in volume expansion equal to 0·1% that occurred in the case of the non-added sample, no change in size was observed in the 2 wt-%TiO_2 added sample either before or after sintering and a firing shrinkage occurred equal to 0·4%, and 0·6% that occurred upon addition of 3 and 4 wt-%TiO_2 respectively.

Variation of volume in the change (%) with TiO_2, the (%) addition is given in Fig. 2.

The samples in the series of the T0 to T4 test result demonstrated that the (T2) 2 wt-%TiO_2 addition was the optimum additive ratio.

Table 3 shows that the 2 wt-% addition of the TiO_2 additive was highly effective on the densification behaviour of the castable. Using the 2 wt-% addition of the TiO_2 increased the bulk density of the brick from 3·02 to 3·10 g cm^{-3} at 1600°C. Moreover, the CCS of the castable increased with the 2 wt-% amount of the TiO_2 addition, while apparent porosity and water absorption decreased at each sintering temperature.

Phase analysis

The physical properties of the castables that were supported by the X-ray diffraction analysis of the samples taken from the T0 *to* T4 are given in Fig. 3*a–e*.

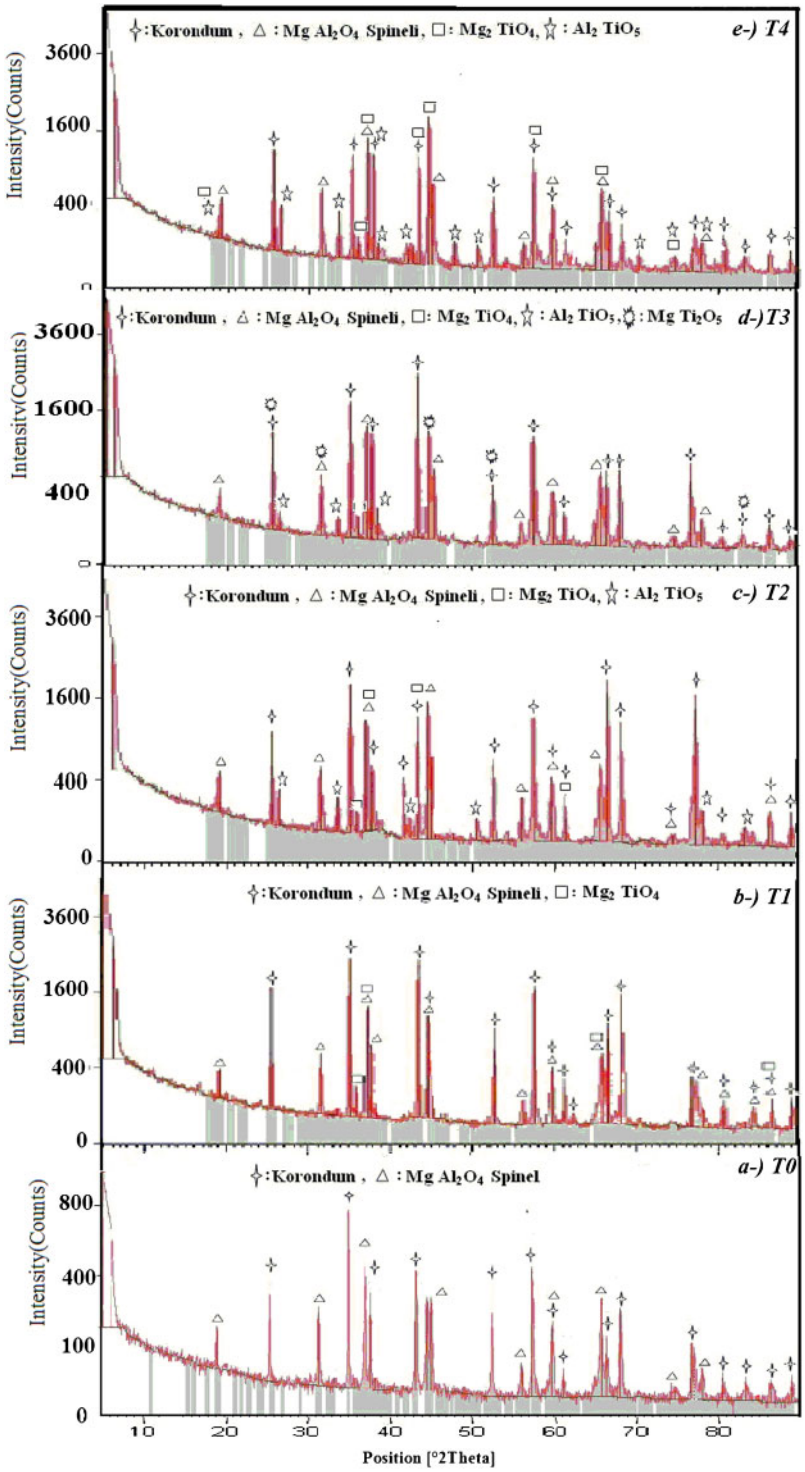
Figure 3 indicates that the spinel phase's intensity of the T2 sample is greater than that of the T0 sample. The Mg_2TiO_4 and Al_2TiO_5 phases were formed with the

Table 2 Particle size and mass contents of castable/wt-%

Raw materials	Particle size/mm	T0/wt-%	T1/wt-%	T2/wt-%	T3/wt-%	T4/wt-%
Tabular alumina	1–6	37·20	37·20	37·20	37·20	37·20
Tabular alumina	0·04–1	33·60	33·60	33·60	33·60	33·60
MgO	0·04–0·1	2·00	2·00	2·00	2·00	2·00
MgO	−0·04	4·00	4·00	4·00	4·00	4·00
Tabular alumina	−0·04	8·20	7·20	6·20	5·20	4·20
Reactive Alumina	−0·04	7·00	7·00	7·00	7·00	7·00
Calcined Alumina	−0·04	4·97	4·97	4·97	4·97	4·97
α-500	−0·04	3·00	3·00	3·00	3·00	3·00
TiO_2	–	–	1·00	2·00	3·00	4·00
Dispersant	–	0·03	0·03	0·03	0·03	0·03

Table 3 Physical and mechanical properties of containing TiO_2 and free from additive castables

	T0		T1		T2		T3		T4	
Physical properties	1500°C	1600°C	1500°C	1600°C	1500°C	1600°C	1500°C	1600°C	1500°C	1600°C
Water absorption/%	6·38	6·24	6·25	5·32	6·12	5·10	6·16	5·42	6·32	5·49
Apparent porosity/%	19·24	18·70	18·83	16·4	18·40	15·70	18·53	16·75	18·88	16·79
Bulk density/g cm^{-3}	3·02	3·02	3·01	3·08	3·01	3·10	3·00	3·10	3·00	3·05
Cold crushing strength/MPa	115	167	151	254	220	275	175	200	147	193



a T0; *b* T1; *c* T2; *d* T3; *e* T4

3 X-ray diffraction analysis of free from additive T0 and TiO_2 addition of castables at 1600°C

2 wt-% TiO_2 addition. These phases are responsible for improving the physical properties of the castable.

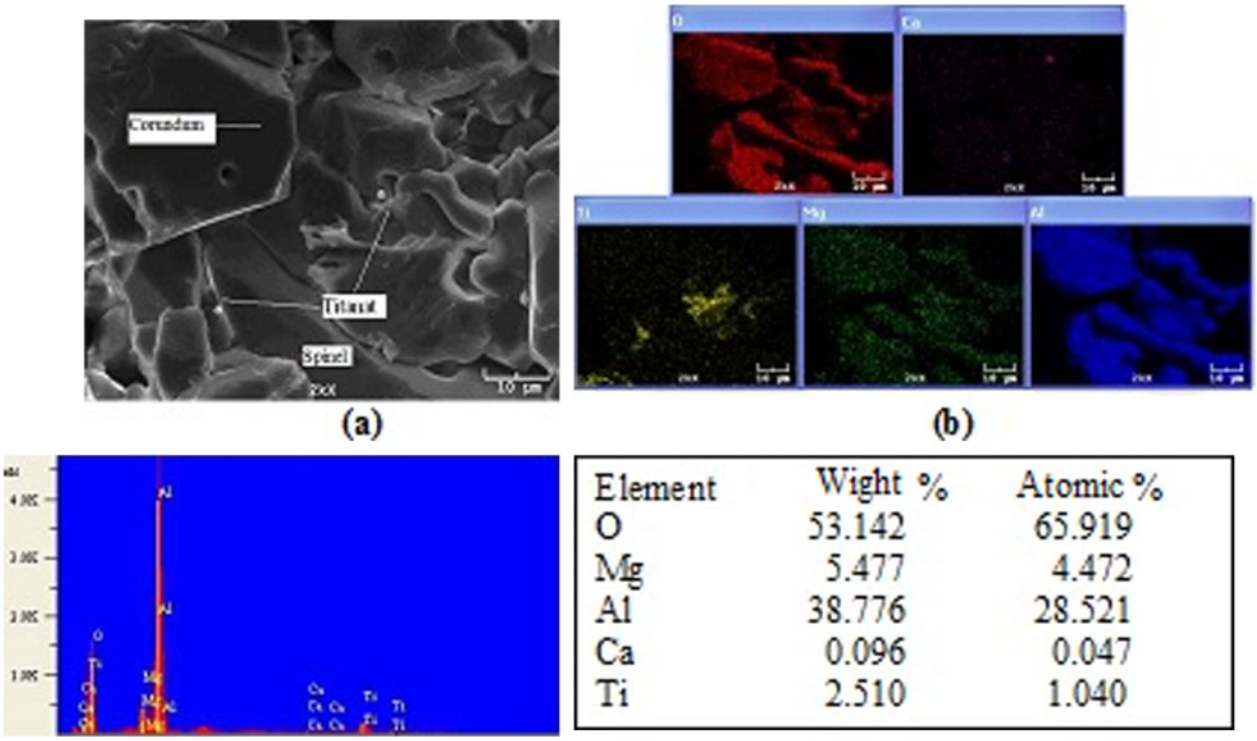
The $MgTi_2O_5$ transition phase defined by Buscaglia was determined in the 3 and 4 wt-% TiO_2 added castables sintered at 1600°C. It was observed that the values for the apparent porosity (%) and water absorption (%) increased, while the CCS decreased.

As seen in Fig. 2, firing shrinkage equal to 0·4 and 0·6% occurred in the 3 and 4 wt-%TiO_2 added castables respectively, while any change in volume did not occur in the 2 wt-% TiO_2 blended castables.

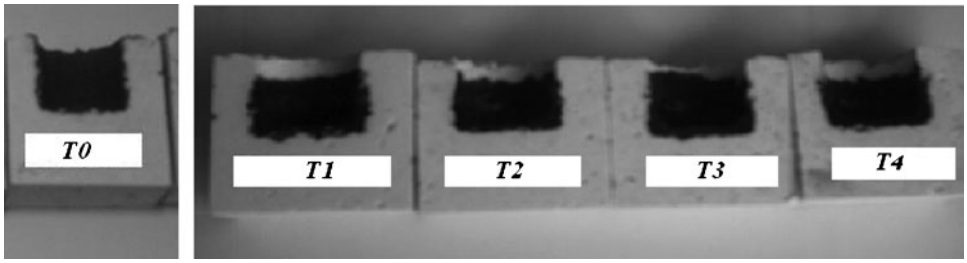
According to Table 3 and Fig. 2, it may be said that inverse spinel Mg_2TiO_4[21] has a positive effect on the physical properties of refractory castables, while the presence of $MgTi_2O_5$ transition phase determined in the 3–4 wt-% TiO_2 blended refractory castables has a negative effect.

Microstructural analysis

According to the view of the 2 wt-%TiO_2 added sample under an electron microscope as seen in Fig. 4*a*, magnesium aluminate spinel ($MgAl_2O_4$) with angular



4 Image (SEM) of *a* general image (×2000), *b* element map and *c* EDS analysis of 2 wt-% TiO_2 T2 addition of castable at 1600°C



5 Slag penetration area images of samples at 1600°C

shaped big crystals are tabular alumina. Tabular alumina consists of the corundum phase and includes large closed pores. Figure 4*b* shows the element map of the sample. It shows the general distribution of the elements of Mg, Al, Ti, O and Ca in the sample, while Fig. 4*c* shows EDS analysis of this zone.

Slag corrosion resistance (crucible method)

Ladle slag from the steel plant supplied from the Steel Plant of Erdemir Inc. was utilised in the corrosion tests of the castable samples. The chemical composition of this slag is given in Table 4. The slag that is composed mainly of $CaO–Al_2O_3–SiO_2$ contains 17·66% iron solution ($FeO+Fe_2O_3$). It was granulated and sifted in a 100 μm sieve. The powdered slag under the sieve was separated in order to be used in the corrosion test.

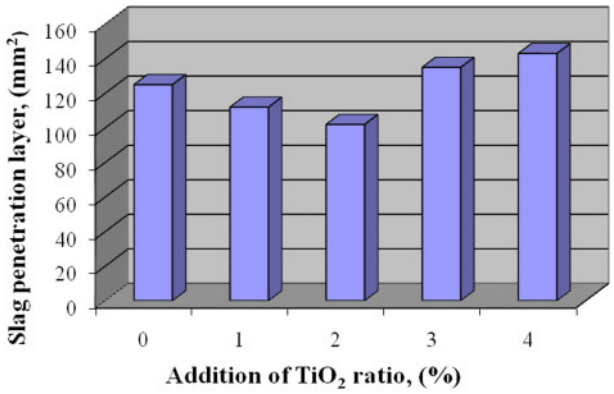
Slag charge was applied to the inside of the castable crucible pot samples prepared according to the DIN 51069 and sintered at 1600°C for 4 h in a Naber Therm (Germany) type furnace at a heating rate of 10°C min^{-1}. The castable samples, which had interacted with the slag, were cut as stated in the DIN 51069, and their corrosion surfaces were examined.

An intense slag region comprising dissolution and infiltration areas was observed at the interfaces (Figs. 5 and 6). For the comparison of the slag infiltration in the samples T0, T1, T2, T3 and T4, slag infiltration areas were measured with the use of semiquantitative graph measurement paper. As shown in Fig. 6, slag infiltration of castable containing 2 wt-%TiO_2 additive was slightly lower than free from additive (T0).

Figure 7 shows elemental distribution analysis of slag penetration layer along the line in T2 castable, and Fig. 8 shows the EDS point analysis extending from the slag contact zone of the same region to the inner sections of the refractory and gives the corresponding chemical

Table 4 Chemical composition of ladle slag (C/S=2·29)/%

	FeO/Fe_2O_3	SiO_2	MnO	Al_2O_3	CaO	MgO	P_2O_5	S	Na_2O	K_2O	TiO_2	Cr_2O_3
Wt-%	17·66	14·32	4·62	14·02	32·87	7·01	0·617	0·221	0·001	0·107	0·483	0·114



6 Slag penetration areas of samples at 1600°C

composition of sample T2. Results of EDS in the figure are taken from the corroded zone (hot zone), uncorroded refractory zone (cold zone) and border between the hot and cold zone (border zone).

Castables with high alumina, including synthetic or *in situ* $MgAl_2O_4$ spinel's

$$MgO{\cdot}Al_2O_3 + (n-1)Al_2O_3 \rightarrow MgO{\cdot}nAl_2O_3 \quad (1)$$

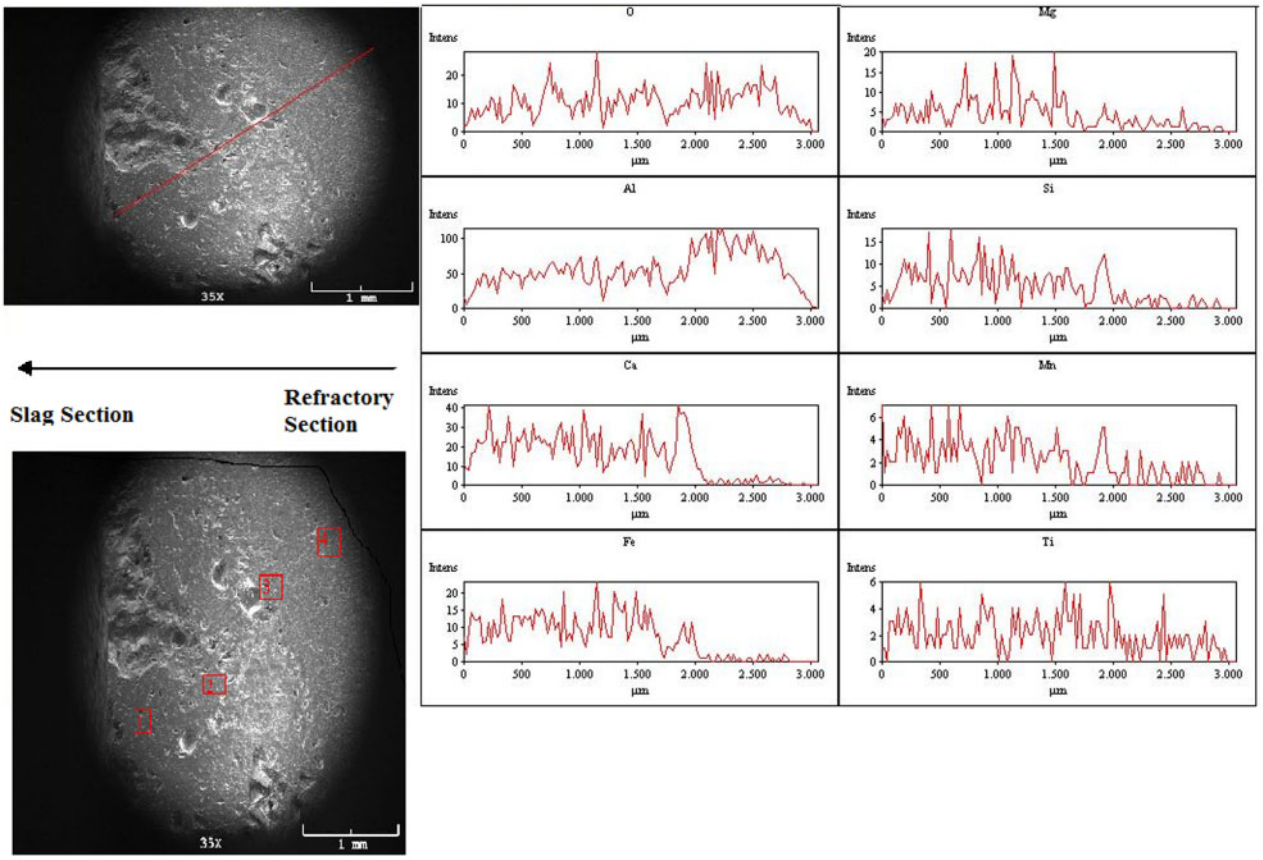
It has a lattice structure that has cation vacancies, as is due to reaction (1). These vacancies allow easy infiltration of Fe and Mn ions, so that the stability of the structure is protected and it resists very well against the slag attacks,[22] i.e. the concentration of Fe and Mn decreases and their expansion to deeper areas is hindered.

On the other hand, 2% TiO_2 assisted in the formation of liquid phases, and it also formed solid solutions with MgO and Al_2O_3. It also assisted in the formation of extensive spinel phases, which remained stable at all the firing temperatures under the experimental conditions.[23] In addition to the above functions, a portion of TiO_2 acts as nucleating agent, recrystallising some part of the liquid phase at higher temperatures to form secondary spinel phases. The grain sizes of spinel phases were found to decrease with the increase in TiO_2 additives in the batches.[24] TiO_2 acted as grain boundary stabiliser for spinel grains, with the formation of reduced sized grains. Consequently, with the addition of 2 wt-%TiO_2, change in volume has not been determined, and the trend was observed to be quite prominent at 1600°C, which was the highest sintering temperature under the experimental condition. This clearly indicated a positive influence of TiO_2 on the sintering process.

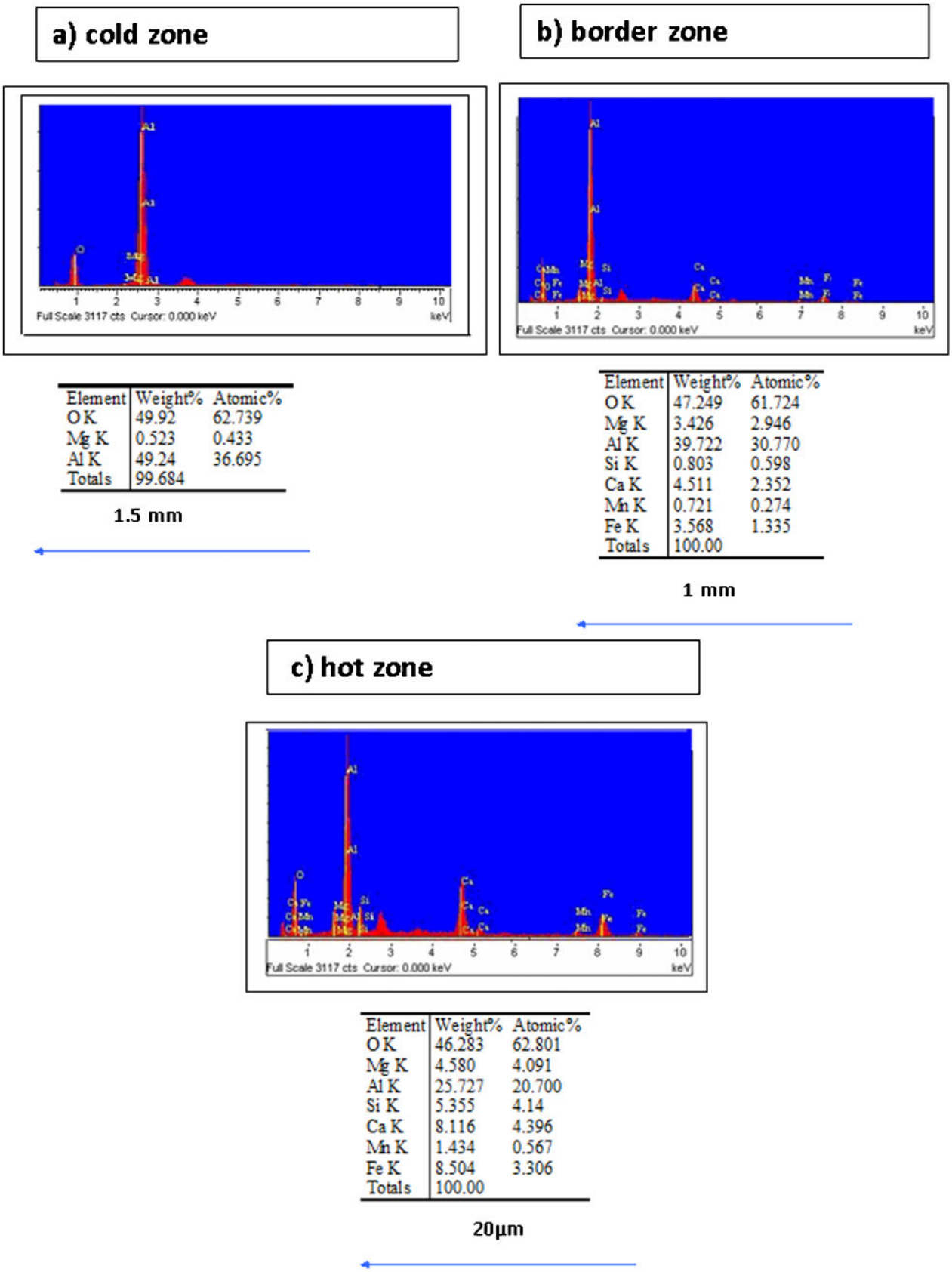
When the results of EDS analysis is examined, the influence of Fe, Mn, Ca and Si ions likely to diffused from the slag in hot zone, is clearly seen. This diffusion continues until the border zone.

Mori *et al.*[25] explained that the slag is composed mainly of CaO–FeO–SiO_2, CaO in the slag reacts primarily with Al_2O_3 to form CaO–Al_2O_3 compounds, while the FeO forms solid solution in the spinel. Slag composition moves to a SiO_2 rich composition, and the penetration layer rises. However, liquid phase viscosity raises, and hence, further penetration is blocked.

According to the EDS analysis results given in Fig. 8, the amount of Si, Ca, Mn and Fe in the 2 wt-% TiO_2 (T2) addition to the castable in the slag section is higher, but the infiltration length of the slag is lower. It is explained that in the situ formation of the $MgAl_2O_4$ spinel, Mg_2TiO_4 inverse spinel and Al_2TiO_5 tialite (pseudobrookite) phases enhance the resistance against the slag corrosion.



7 Elemental distribution analysis of slag penetration layer along line in 2 wt-%TiO_2 T2 addition of castable



8 *a–c* energy dispersive spectrometer point analysis of slag penetration layer of 2 wt-% TiO_2 T2 addition of castable (marked in Fig. 7)

However, the amount of Si, Ca, Mn and Fe in 2 wt-% TiO_2 (T2) addition to the castable in the penetration section decreased as seen in Fig. 8.

In this study, it was claimed that $MgAl_2O_4$ spinel formation was supported with the TiO_2 addition; in this way, slag penetration on the surface of the castable was

blocked. On the basis of the EDS analyses as given in Fig. 8, in the sample T2, slag infiltration is quite low.

As a result of the SEM-EDS analysis given in Fig. 8*b*, it is seen that a ~1 mm slag diffuses from hot zone to cold zone

Conclusions

1. All of the physical properties of the castable as shown above in Table 3 improved using 2 wt-% TiO_2 (T2) addition at 1600°C.

2. It was defined that $MgAl_2O_4$ spinel and Mg_2TiO_4 inverse spinel occurred at the 1 wt-% TiO_2 addition of the castables. However, formation of the Al_2TiO_4 was not observed (Fig. 3*a*).

3. $MgAl_2O_4$ spinel and Mg_2TiO_4 inverse spinel structure are also determined, as well as the formation of Al_2TiO_5 in 2 wt-% TiO_2 addition to the castables (Fig. 3*b*).

4. As seen in Table 3, the formation of Al_2TiO_5 has a positive effect on the physical properties of the castables.

5. The Mg Ti_2O_5 transitional phase causes a decrease in volume for the 3–4 wt-% TiO_2 addition to the castables. Therefore, the physical properties of the castables were affected negatively (Fig. 2).

6. In this study, it was mooted that the slag penetration on the surface of the castable was blocked. These results were compared with Kalpaklı;[20] and the slag infiltration of the hot zone decreased from 40 to 20 mm (Fig. 8).

Acknowledgements

I would like to thank the Superateş Refractories Company for their support throughout this investigation. This study was supported by YTÜ BAPK project no. 28-07-01-03 as an industrial project.

References

1. S. Zhang and W. E. Lee: 'Spinel-containing refractories', in 'Refractories handbook', 215–257, New York, Marcel Dekker Inc.
2. S. Maitra, S. Das and A. Sen: 'The role of TiO_2 in the densification of low cement Al_2O_3–MgO spinel castable', *Ceram. Int.*, 2007, **33**, 239–243.
3. H. R. Fernandes, D. U. Tulyaganov, J. M. F. Ferreira: 'The role of P_2O_5, TiO_2 and ZrO_2 as nucleating agents on microstructure and crystallization behavior of lithium disilicate-based glass', *J. Mater. Sci.*, 2013, **48**, 765–773.
4. Y. Kalpaklı, S. Gökmen and S. Özgen: 'Effect of binder type and other parameters in synthesis of magnesite chromite refractories from process waste', *J. Eur. Ceram. Soc.*, 2002, **22**, 755–759.
5. D. P. H. Hasselman: 'Thermal stress resistance parameters for brittle refractory ceramics', *Ceram.Bull.*, 1970, **49**, (12), 1033–1037.
6. R. D. Skala, D. Li, M. A. Low: 'Diffraction, structure and phase stability studies on aluminium titanate', *J. Eur. Ceram. Soc.*, 2009, **29**, 67–75.
7. R. Naghizadeh, H. R. Rezaie and F. Golestani-fard: 'The influence of composition, cooling rate and atmosphere on the synthesis and thermal stability of aluminum titanate', *Mater. Sci. Eng. B*, 2009, **B157**, 20–25.
8. C. G. Aneziris, E. Pfaff and H. R. Maier: 'Ceramics materials in the system ZrO_2–TiO_2–Al_2O_3 for applications in the ferrous and nonferrous metallurgy', *Key Eng. Mater.*, 1997, **132–136**, 1829–1833.
9. C. G. Aneziris, W. Scharfl and B. Ullrich: 'Microstructure evaluation of Al_2O_3 ceramics with Mg-PSZ and TiO_2 additions', *J. Eur. Ceram. Soc.*, 2007, **27**, 3191–3199.
10. Y. Ohya and Z. Nakagawa: 'Grain boundary microcracking due to thermal expansion anisotropy in aluminium titanate ceramics', *J. Am. Ceram. Soc.*, 1987, **70**, (8), C184–C186.
11. A. M. Segadeas, M. R. Morelli and R. G. A. Kaminami: 'Combustion synthesis of aluminium Titanate', *J. Eur. Ceram. Soc.*, 1998, **18**, 771–781.
12. T. Korim: 'Effect of Mg^{2+} and Fe^{3+} ions on formation mechanism of aluminium titanate', *Ceram. Int.*, 2009, **35**, 1671–1675.
13. A. Tsetsekou: 'A comparison study of tialite ceramics doped with various oxide material and tialite–mullite composites: microstructural, thermal and mechanical properties', *J. Eur. Ceram. Soc.*, 2005, **25**, 335–348.
14. V. Buscaglia, F. Caracciolo and M. Lenoi: 'Synthesis, sintering and expansion of $Al_{0.8}Mg_{0.6}Ti_{1.6}O_5$: a low-thermal-expansion material resistant to thermal decomposition' *J. Mater. Sci.*, 1997, **32**, 6525–6531.
15. V. Buscaglia, P. Nanni and G. Battilana: 'Reaction sintering of aluminium titanate. I: effect of MgO addition', *J. Eur. Ceram. Soc.*, 1994, **13**, 411–417.
16. L. Giordano, M. Viviani, C. Bottino, M. T. Buscaglia, V. Buscaglia and P. Nanni: 'Microstructure and thermal expansion of Al_2TiO_5–$MgTi_2O_5$ solid solution obtained by reaction sintering', *J. Eur. Ceram. Soc.*, 2002, **22**, 1811–1822.
17. M. D. Xirouchakis: 'Pseudobrookite-group oxide solutions and baaltic melts', *Lithos*, 2007, **95**, 1–9.
18. Y. X. Huang and A. M. R. Senos: 'Effect of the powder precursor characteristics in the reaction sintering of aluminum titanate', *Mater. Res. Bull.*, 2002, **37**, 99–111.
19. R.-G. Duan, G.-D. Zhan, D. J. Kuntz, B. H. Kear and A. K. Mukherjee: 'Spark plasma sintering (SPS) consolidated ceramic composites from plasma-sprayed matastable Al_2TiO_5 powder and nano-Al_2O_3, TiO_2 and MgO powders', *Mater. Sci. Eng. A*, 2004, **A373**, 180–186.
20. Y. Kalpaklı: 'Comparative study for physical properties and corrosion mechanism of synthetic and *in situ* $MgAl_2O_4$ spinel formation zero cement refractory castables', *Ironmaking Steelmaking B*, 2010, **34B**, (6), 414–424.
21. A. Golubovic and M. Radovic: 'The growth of Mg_2TiO_4 single crystals using a four-mirror Furnace', *J. Serb. Chem. Soc.*, 2011, **76**, (11), 1561–1566.
22. S. Yılmaz: 'Corrosion of high alumina-spinel castables by steel ladle slag', *Ironmaking Steelmaking*, 2006, **33**, (2), 151–156.
23. A. S. Berezhoni and N. V. Gulko: 'Phase diagram of the system MgO–Al_2O_3–TiO_2', *Ukrain. Khim. Zhur.*, 1955, **2192**, 162.
24. B. D. Cullity: 'Elements of X-ray diffraction', 388–392; 1959, Boston, MA, Addison-Wesley Publishing Company Inc.
25. J. Mori, W. Watanabe, M. Yoshimura, Y. Oguchi and T. Kawakami: 'Material design of monolithic refractories for steel ladle', *Bull. Am. Ceram. Soc.*, 1990, **69**, (7), 1172–1176.